Ore Geology Reviews 74 (2016) 139–150

Contents lists available at ScienceDirect

Ore Geology Reviews

journal homepage: www.elsevier.com/locate/oregeorev

Iron isotope fractionation during skarn-type alteration: Implications for metal source in the Han-Xing iron skarn deposit

Bin Zhu [a,b,*], Hong-Fu Zhang [a,*], Xin-Miao Zhao [a], Yong-Sheng He [c]

[a] State Key Laboratory of Lithospheric Evolution, Institute of Geology and Geophysics, Chinese Academy of Sciences, Beijing 100029, China
[b] School of Earth Science, University of Chinese Academy of Sciences, Beijing 100049, China
[c] State Key Laboratory of Geological Processes and Mineral Resources, China University of Geosciences, Beijing 100083, China

ARTICLE INFO

Article history:
Received 8 May 2015
Received in revised form 19 October 2015
Accepted 1 November 2015
Available online 4 November 2015

Keywords:
Fe isotope
Skarn-type alteration
Fe skarn deposit
Isotopic fractionation
Metal source

ABSTRACT

The Han-Xing iron mineralization in the central North China Craton is a typical Fe skarn deposit associated with altered diorites. Here we report the Fe isotopic compositions of whole rocks and mineral separates from this deposit with a view to evaluate the Fe isotope fractionation during the formation of Fe skarn deposit, and to constrain the metal source. The Fe isotopes show a large variation both in whole rocks and mineral separates. Altered diorites show a wide range in δ^{56}Fe values (−0.07‰ to +0.21‰ relative to the Fe isotope standard IRMM-014) which positively correlate with their TFe_2O_3/TiO_2 ratios (Fe_2O_3 and FeO calculated as TFe_2O_3). The positive correlation indicates that heavy Fe isotopes were preferentially leached from diorites during the skarn-type alteration. Among the metallic minerals, pyrite and pyrrhotite are isotopically heavier (+0.12‰ to +0.48‰) than the magnetite (+0.07‰ to +0.21‰). Fe isotope fractionation between mineral pairs demonstrates that magnetite did not attain Fe isotopic equilibrium with pyrite and pyrrhotite, whereas pyrite and pyrrhotite might have attained isotopic equilibrium. Petrological observations and major element data also suggest that iron was leached from the diorites during the skarn-type alteration. If the leached iron provides the main Fe budget of the Han-Xing Fe skarn deposit, magnetite in ores would be isotopically heavier than the unaltered diorite. However, our results are in contrast with the magnetite being isotopically lighter than the unaltered diorite. This suggests that the major Fe source of the Han-Xing Fe skarn deposit is not from the leaching of diorites, and might be from magmatic fluid which is isotopically lighter than the silicate melt. Our data demonstrate that Fe isotopes can be used as important tracers in deciphering the metal source of Fe skarn deposits.

1. Introduction

Tracing the source of metals is a key issue in investigations related to the genesis of ore deposits. Light stable isotopes such as H, C, O, N, and S have been used to trace the origin of metal deposits (e.g., Jia and Kerrich, 1999; Ohmoto, 1972; Rye, 1966; Sheppard et al., 1971; Taylor, 1974). However, these elements are not metallogenic elements themselves and have different isotopic signatures under different tectonic settings (Hedenquist and Lowenstern, 1994), which makes it difficult to decipher the metal source. For example, the hydrogen and oxygen isotopic compositions of hydrothermal minerals from Cu porphyry deposit often show a mixed feature of magmatic and meteoric water, whereas sulfur isotope records the isotopic composition of mantle sulfur. Thus none of these proxies provide direct information on the source of copper. Therefore, metal stable isotopes (e.g., Fe, Mg, Cu, Zn, Cr and Mo) have emerged as more precise tracers. As an important rock-forming and metallogenic element, iron occurs in either reduced ferrous iron or oxidized ferric iron in nature. The differences in the behavior of iron with different redox states and significant isotopic variations make Fe isotope useful for tracing the iron geochemical cycle (Beard and Johnson, 2004).

The application of Fe isotopes to trace metal source is still debated, due to lack of precise information on the Fe isotope fractionation during metallogenic processes. In a study of the Grasberg Cu–Au porphyry deposit, Graham et al. (2004) found that Fe isotopic compositions of pyrite and chalcopyrite from the Grasberg Igneous Complex and the skarn overlapped, based on which they invoked a genetic relationship. However, this conclusion can be debated since Fe isotopes can fractionate during many processes (e.g., Bullen et al., 2001; Icopini et al., 2004; Skulan et al., 2002; Teng et al., 2008; Cheng et al., 2015). Markl et al. (2006) suggested that Fe isotopes are not suitable to derive information on metal sources as the isotopic composition is strongly dependent on the characteristic of fluid and precipitation history. However, in another case, Wang et al. (2011) studied the Fe isotopic fractionation of the metallogenic processes in the Xinqiao Cu–S–Fe–Au deposit and excluded the sedimentary strata as the iron source.

* Corresponding authors at: Institute of Geology and Geophysics, Chinese Academy of Sciences, China.
E-mail addresses: binz@mail.iggcas.ac.cn (B. Zhu), hfzhang@mail.iggcas.ac.cn (H.-F. Zhang).

http://dx.doi.org/10.1016/j.oregeorev.2015.11.001
0169-1368/

As the largest skarn deposit type on the globe, Fe skarn deposits occur in different times and geological settings (Meinert et al., 2005). In China, Fe skarn deposits constitute the dominant source of high-grade iron ores (Zhang et al., 2014a). The various models proposed for the metal sources of Fe skarn deposits can be grouped into three: 1) recycling of pre-existing ore deposits (e.g., Johnson et al., 1990; Wang et al., 1981); 2) alteration of associated igneous rocks (e.g., Feng, 1998; Zheng et al., 2007); and 3) products of magmatic hydrothermal system (e.g., Shimazaki, 1980). Apart from a few examples for skarn formation through the recycling of pre-existing ore deposits, most researchers favor the second and third models above (e.g., Hedenquist and Lowenstern, 1994; Jin et al., 2015; Xie et al., 2015; Zhang et al., 2014b). In this paper, we report Fe isotopic compositions of altered diorites, limestone and metallic minerals from the Han-Xing Fe skarn deposit as well as the major element compositions of altered diorites, in an attempt to evaluate the behavior of elemental iron and iron isotopes during the formation of Fe skarn deposit, as well as to constrain the Fe source. Our results demonstrate that heavy Fe isotopes were preferentially leached from the diorites during the skarn-type alteration and the main Fe budget was derived from magmatic fluid.

2. Geological setting

2.1. Regional geology

The NCC is a collage of Archean microcontinents which were assembled into major crustal blocks at the end of Archean followed by rifting-subduction-accretion collision that culminated by end Paleoproterozoic, building the fundamental cratonic architecture (Santosh et al., 2015; Yang and Santosh, 2015; Yang et al., 2015; Zhai and Santosh, 2011; Zhai, 2014; Zhao and Zhai, 2013), The Han-Xing iron district is located in the central part of the NCC (Fig. 1A). The basement rocks in this region are mainly composed of tonalite-trondhjemite-granodiorite (TTG) gneisses and amphibolites, the protoliths which formed during Meso–Neoarchean and were metamorphosed during late Paleoproterozoic coeval with the final cratonization of the NCC (Zhai and Santosh, 2011). Regionally, the sedimentary rocks in this area are dominated by Cambrian–Ordovician carbonates in the western part and Carboniferous–Permian clastic rocks in the eastern part (Fig. 1B). Mesozoic magmatic rocks intruded into the Precambrian basement as well as the sedimentary cover. Previous studies proposed that the source magmas of these intermediate intrusive rocks with zircon SHRIMP U-Pb ages of 126–138 Ma were generated by crust-mantle interaction (Chen et al., 2008).

2.2. Ore geology

The samples for this study were collected from the Wu'an iron cluster region which is composed of several iron deposits, about 10 km away from the Wu'an County, Hebei Province (Fig. 1B). The dominant basement rocks in this region belong to the Archean Zanhuang Complex, intruded by the Mesozoic intermediate plutons of monzonite, monzodiorite, diorite, and quartz–diorite. The major sedimentary unit associated with the deposit is the Middle Ordovician Majiagou limestone.

The main ore-controlling structure is a set of NNE extensional faults. Most of the Fe deposits formed around the Wu'an fault basin (Li, 1986) (Fig. 1 B). Ore bodies occur as complex lenses with serrated and interspersed features typically at the contact zone of the dioritic plutons and the Majiagou limestone. The well developed alteration zone between the dioritic plutons and limestone can be further divided into five zones as: altered diorite, endoskarn, magnetite ore, exoskarn and marmorized limestone zone. In general, the endoskarn shows a wider

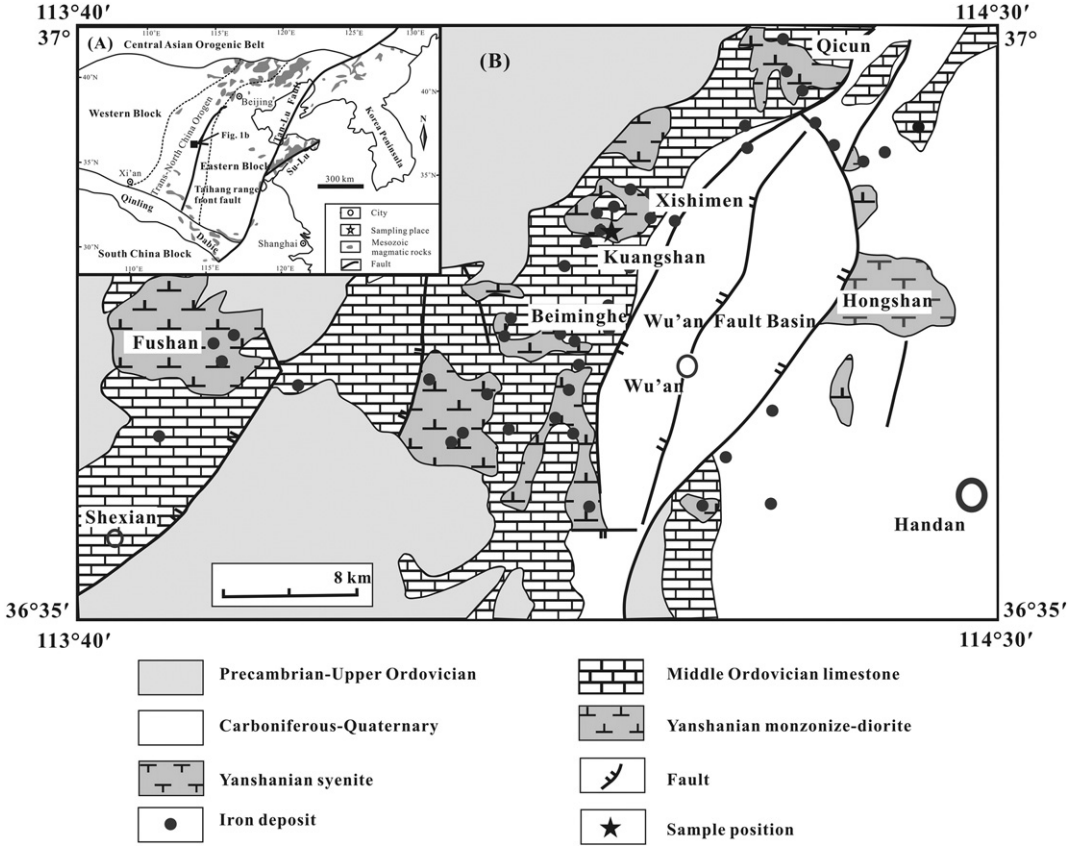

Fig. 1. (A) Simplified geological map showing major tectonic subdivisions of the North China Craton (NCC) with an emphasis on the distribution of Mesozoic magmatic rocks (after Zhao et al., 2005; Qian and Hermann, 2010). (B) Local geological map of the Wu'an iron deposit (modified from Shen et al., 2013).

distribution than the exoskarn and the diopside-type skarn dominates the Fe skarn deposit. The ore minerals are dominated by magnetite with minor hematite, pyrite, pyrrhotite and chalcopyrite. Skarn minerals mainly include diopside, garnet, epidote, actinolite, phlogopite and serpentine. The marmorized limestone at the external contact zone often has been brecciated or altered by chlorite. The content of magnetite in ores varies from 40 to 90% (Fig. 2).

3. Sampling and analytical methods

3.1. Sampling

Six diorites with various degrees of skarn-type alteration were collected from the altered diorite zone for major elements and Fe isotope analyses. With increasing alteration, the color of diorites becomes lighter (Fig. 2). Samples WA12-14 and WA12-07 are weakly altered diorites which mainly consist of plagioclase, amphibole, K-feldspar, and pyroxene with minor biotite and quartz. Magnetite, allanite, sphene, apatite and zircon occur as accessory minerals. Samples WA12-08 and WA12-31 are moderately altered diorites, where most amphibole has been replaced by diopside, and K-feldspar was altered to albite. Samples WA12-13 and WA12-23 are intensely altered diorites, which are close to the endoskarn and mainly composed of albite, K-feldspar and minor pyroxene without amphibole (Table 1 and Fig. 2). The "diorite skarn-type alteration" in this study refers to the whole alteration effect on the diorite during the formation of skarn deposit, whereas in many previous studies of the Han-Xing skarn deposit, researchers used "albitization" to represent the "diorite skarn-type alteration" following the observation of albite formation during this process. The syenite occurring next to the location of sample WA12-14 was also analyzed for comparison, which is composed of K-feldspar (60–80%), plagioclase (15–20%), amphibole (5%), biotite (5%), minor quartz and clinopyroxene. Two limestones have been marmorized. All the rocks mentioned above show compact structure without any secondary alteration features after the skarn formation.

Amphibole in diorites was altered to aggregates of diopside, albite, biotite and magnetite during the skarn-type alteration (Fig. 3A). The newly-formed magnetite is associated with the diopside (Figs. 3A-B

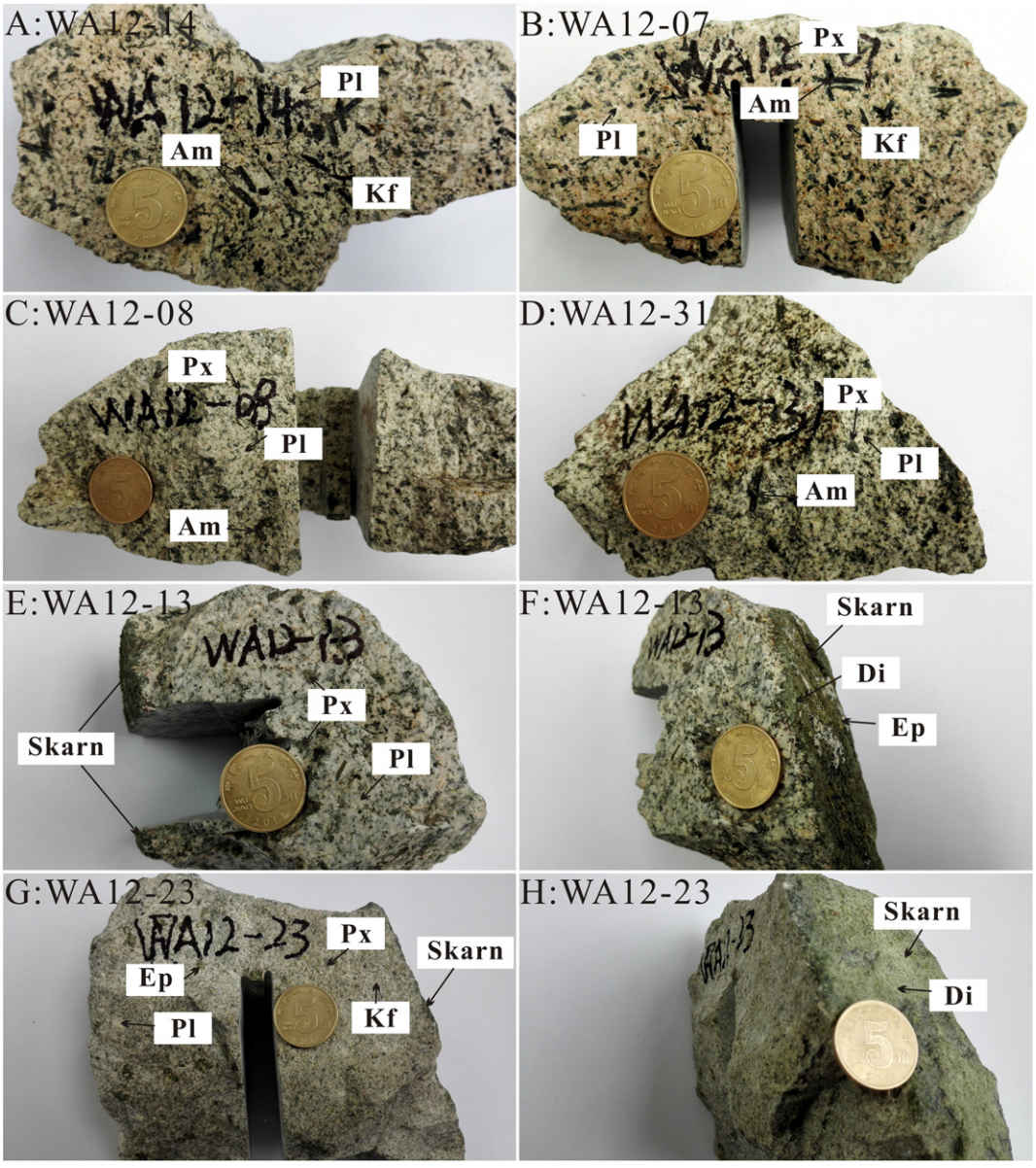

Fig. 2. Hand specimens of altered diorites and ores from the Han-Xing Fe skarn deposit. Abbreviations: Am-amphibole; Px-pyroxene; Di-diopside; Mgt-Magnetite; Kf-K-feldspar; Pl-plagioclase; Ep-epidote; Py-pyrite; Cal-calcite.

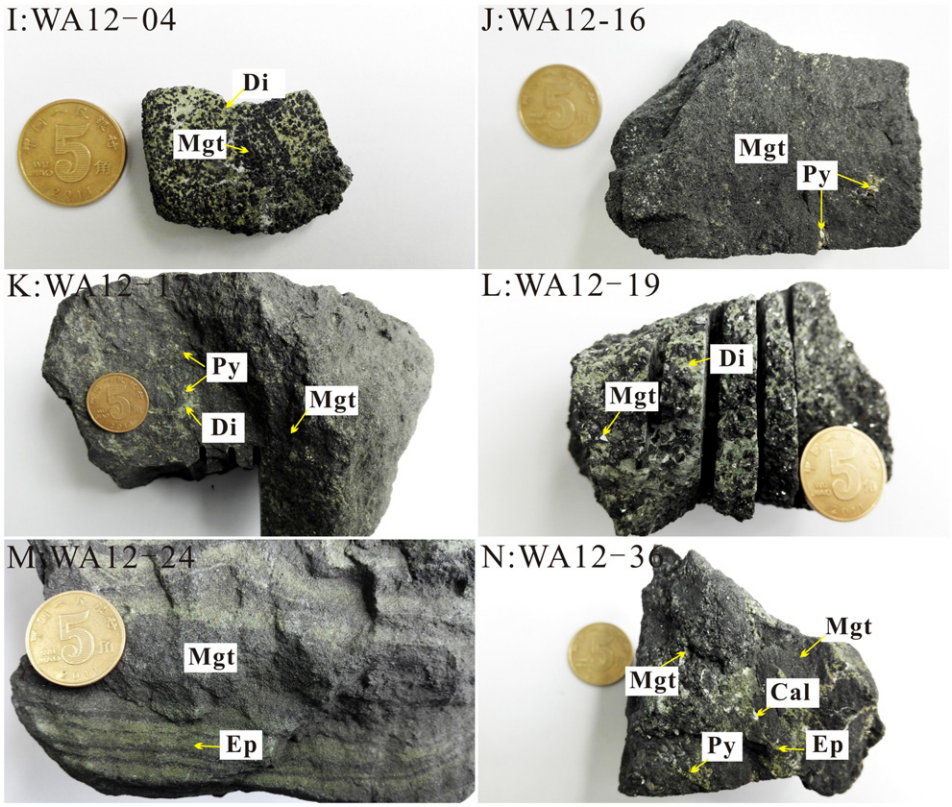

Fig. 2 (*continued*).

and 4). With the increase in the degree of alteration, the newly-formed minerals (diopside and biotite) were progressively transferred to albite. Meanwhile, both the newly formed hydrothermal magnetite and the pre-existing magmatic magnetite were dissolved from the altered diorites (Fig. 3C–D). In some cases, amphibole was completely replaced by albite with only the preservation of grain morphology.

Thirty ore mineral separates of magnetite, pyrite and pyrrhotite were separated from twelve ore samples for Fe isotope analyses. These ores are mainly composed of magnetite, epidote, diopside and sulfides with minor calcite and serpentine in certain samples. The ores show massive, disseminated, banded and taxitic structures (Table 1 and Fig. 2). Most of the ores are of high grade, with an average of 40–60% Fe.

Magnetite can be divided into two groups: anhedral to subhedral fine magnetite grains in a range of 0.1–0.25 mm and euhedral coarse magnetite grains of 1–4 mm (Figs. 2I–N and 3E–H). Generally, the coarse magnetite coexists with the calcite (Fig. 2N). Pyrite and pyrrhotite are anhedral to euhedral fine or medium grains (0.1–0.5 mm) and mainly exist between the magnetite and gangue minerals, implying that they were formed after the formation of the magnetite and gangue minerals (Figs. 2K and 3G–H).

According to our petrological observations and the fluid inclusions work by Zheng et al. (2007), three stages can be recognized during the formation of Han-Xing Fe skarn deposit. The early stage includes the alteration of diorites and prograde skarn stage (resulting in the formation of garnet and diopside). The middle retrograde skarn stage is also the main mineralization stage, at which the magnetite, biotite and epidote were formed. The late stage is characterized by the chlorite-calcite-sulfide assemblage.

3.2. Analytical methods

3.2.1. Major elements

Whole rocks were powdered with an agate mill to 200 mesh and 0.5 g powders were mixed with 5 g of $Li_2B_4O_7$. A glass slice was formed via fusion. Major elements were determined using a Phillips PW 2400 sequential X-ray fluorescence spectrometer (XRF) at the Institute of Geology and Geophysics (IGG), Chinese Academy of Sciences. The analytical precision and accuracy is better than ±2% for major oxides. Loss on ignition (LOI) was measured after heating to 1000 °C. The FeO was determined by Redox Titration using $KMnO_4$ solution and the analytical precision is estimated to be <0.5%.

The analyses of major elements of rock-forming minerals and backscattered electron images were performed on a JEOL JXA-8100 microprobe at the IGG. The accelerating voltage, beam current, spot diameter and peak counting time for electron microprobe (EMP) analysis were 15 kV, 10 nA, 5 μm and 20 s, respectively.

3.2.2. Fe isotopes

The chemical purification of Fe was carried out in the Isotope Geochemistry Lab at the IGG. Approximately 30 mg whole rock powders were weighted into a Teflon beaker and dissolved in a mixture of 1.5 ml ultrapure concentrated HF and 0.5 ml ultrapure HNO_3. For mineral separates, 3 to 7 mg powders were dissolved in a mixture of 2 ml ultrapure concentrated HCl and HNO_3. After complete dissolution, the solution was evaporated to dryness and HF was eliminated. Following this, 0.5 ml HCl was added and then evaporated to dryness twice in order to convert the cation to chloride-form. Then added 1 ml purified 7 M HCl to resolve. Finally iron was separated using AGMP-1 anion exchange resin (200–400 mesh) in HCl medium. Detailed procedures were reported in Zhu et al. (2002).

Fe isotope measurement was conducted by a Thermo-Finnigan Neptune Plus MC-ICPMS in the Isotope Geochemistry Lab, China University of Geosciences (Beijing), at "medium" mass resolution mode (MR). The instrument mass bias was corrected by the sample-standard bracketing (SSB) method. Data were reported in the commonly used δ notation ($\delta^{i}Fe = [(^{i}Fe/^{54}Fe)_{sample}/(^{i}Fe/^{54}Fe)_{standard} - 1] * 1000$, where i is 56 or 57 and $(^{i}Fe/^{54}Fe)_{standard}$ is an average of the bracketing two standards relative to IRMM-014. The standard-sample sequences were

Table 1
Sample description of hand specimens of altered diorites and ores from Han-Xing iron deposit.

Type	Sample	Description
Igneous Rock	WA12-14	Fresh or less altered diorite consists of coarse-grained, euhedral black-green amphibole (20%), plagioclase (50%), K-feldspar (25%), with green pyroxene, biotite and quartz less than 5%.
	WA12-07	Less altered diorite consists of coarse-grained, euhedral black-green amphibole (15%), pyroxene (4%), plagioclase (45%), K-feldspar (30%) with biotite and quartz less than 6%.
	WA12-08	Moderately altered diorite, most amphibole was replaced by pyroxene; consists of euhedral amphibole (5%), pyroxene (10%), plagioclase (70%), K-feldspar (10%) with biotite and quartz less than 5%.
	WA12-31	Moderately altered diorite, most amphibole was replaced by pyroxene; consists of euhedral amphibole (3%), pyroxene (10%), plagioclase (65%), K-feldspar (15%) with biotite and quartz less than 7%.
	WA12-13	Intensively altered diorite, close to the skarn; amphibole was completely altered by pryoxene, consists of pyroxene (10%), plagioclase (70%), K-feldspar (15%), with biotite and quartz less than 5%.
	WA12-23	Most intensively altered diorite, close to the skarn; consists of fine-grained green pyroxene (5%), coarse-grained yellow-green epidote (5%), plagioclase (70%), K-feldspar (20%).
Ores	WA12-01	Magnetite powders, collected from the concentrating mill of Han-Xing deposit, representing the average composition of magnetite of this area.
	WA12-04	Medium-fine grained ore with dense disseminated structure, contains 45% magnetite; gangue minerals consist of diopside, epidote, calcite and minor sulfides.
	WA12-16	Fine-grained ore with massive structure, contains 90% magnetite; gangue minerals consist of epidote, calcite and minor sulfides.
	WA12-17	Fine-grained ore with massive structure, contains 85% magnetite; gangue minerals consist of dioposide, epidote, calcite and minor sulfides.
	WA12-19	Coarse-grained ore with massive structure, contains 50% magnetite; gangue minerals consist of diopside, epidote calcite, quartz and minor sulfides.
	WA12-20	Coarse-grained ore with massive structure, contains 65% magnetite; gangue minerals consist of diopside, epidote calcite, quartz and minor sulfides.
	WA12-24	Fine-grained ore with banded structure, contains 50% magnetite; gangue minerals consist of dioposide, epidote and minor sulfides.
	WA12-33	Fine-grained ore with taxitic structure, contains 40% magnetite; gangue minerals consist of dioposide, epidote and minor sulfides.
	WA12-34	Medium-coarse grained ore with massive structure, contains 45% magnetite; gangue minerals consist of dioposide, epidote, serpentine calcite and minor sulfides.
	WA12-35	Fine-coarse grained ore with massive to taxitic structure, contains 45% magnetite; gangue minerals consist of dioposide, epidote, calcite and minor sulfides.
	WA12-36	Fine-coarse grained ore with massive to taxitic structure, contains 50% magnetite; gangue minerals consist of dioposide, epidote, calcite and minor sulfides.
	WA12-37	Fine-coarse grained ore with massive and taxitic structure, contains 50% magnetite; gangue minerals consist of dioposide, epidote, calcite and minor sulfides.

repeated four times, and the isotopic composition given is an average of repetitive analyses. Errors were preferentially reported as 2se, 95% confidence interval after Dauphas et al. (2009) and He et al. (2015). The external precision and accuracy are estimated to be within 0.04‰ for δ^{56}Fe. Details of the mass spectrometry have been described elsewhere (He et al., 2015).

The USGS standard BCR-2 was processed with the unknown samples to control the data quality. The analytical δ^{56}Fe values (+0.087 ± 0.020‰, 2se) is well agreement with the long-term mean (+0.084 ± 0.029‰, N = 17) from the lab (He et al., 2015) and the recommended value (Craddock and Dauphas, 2011a). A duplicate of sample WA12-37 was processed twice and yields identical result within the quoted uncertainty. All the data yielded a slope of 1.47 ± 0.031 (R^2 = 0.983) in a δ^{57}Fe versus δ^{56}Fe diagram, consistent with the theoretical mass-dependent fractionation value for Fe isotope (Young et al., 2002).

4. Results

4.1. Major elements

Major element data from whole rocks and representative minerals of sample WA12-07 are given in Tables 2 and 3, respectively. The results of altered diorites are consistent with the data reported by Chen et al. (2004). The limited variation in SiO_2 (54–58%), TiO_2 (0.53–0.65%), Al_2O_3 (16–18%), and P_2O_5 (0.32–0.41%) suggests homogeneous composition of these diorites before alteration. In contrast, large variations in MgO (1.7–3.0%), CaO (4.1–7.9%), Na_2O (3.9–7.3%), K_2O (0.73–6.7%), and TFe_2O_3 (2.5–6.7%) indicates that these elements are mobile during diorite alteration. The negative correlations are noted between LOI and TFe_2O_3, CaO and TFe_2O_3, and Na_2O and K_2O (Fig. 5), suggesting that Ca and Na entered into the diorites whereas Fe and K were leached from the diorites during alteration. Both syenite and limestone have low TFe_2O_3 contents.

The FeO (total Fe oxides) of amphibole from sample WA12-07 varies from 13.4% to 15.3%, whereas in the altered products, diopside and albite, the range is from 8.04 to 9.63% and 0.26%, respectively. In addition, the newly formed diopside and albite have lower K_2O than amphibole (Table 3). All above features indicate that Fe and K were leached from the diorites during alteration in mineral scale, consistent with the data from whole rock analyses.

4.2. Fe isotopes

A significant Fe isotopic variation has been observed both for whole rocks and mineral separates (δ^{56}Fe = −0.22‰ to +0.48‰) (Table 4 and Fig. 6).

Altered diorites show a large variation in δ^{56}Fe values (−0.07‰ to +0.21‰) among the investigated samples and the weakest altered diorite (WA12-14) possesses the heaviest Fe isotopic composition. The syenite has a similar δ^{56}Fe value (+0.18‰) with sample WA12-14. Two limestones host the lowest δ^{56}Fe values (−0.22‰ and −0.10‰) falling within the field of sedimentary carbonates (e.g., Craddock and Dauphas, 2011b; Dideriksen et al., 2006).

For mineral separates, significant Fe isotopic features are observed as follows. (1) Large variation in δ^{56}Fe values exists between mineral separates (+0.07‰ to +0.48‰). (2) Fe isotopes fractionated between different minerals. Magnetite has limited and low δ^{56}Fe values (+0.07‰ to +0.21‰). Sulfides (pyrite and pyrrhotite) span a wider range in δ^{56}Fe values (+0.12‰ to +0.48‰) and are isotopically heavier than the magnetite. As a result, a clear sequence in Fe isotopes can be traced among these minerals from individual ore sample with $\delta^{56}Fe_{Py} > \delta^{56}Fe_{Po} > \delta^{56}Fe_{Mgt}$. (3) No discernible difference in Fe isotopic composition between fine and coarse-grained magnetite has been observed.

5. Discussion

5.1. Fe isotope fractionation in diorites during the skarn-type alteration

The marked variation in Fe isotopic compositions of diorite from the Han-Xing skarn deposit suggests significant fractionation of Fe isotopes during the skarn formation processes. The limited variation in immobile elements such as Si, Ti, Al and P (Table 2) demonstrates that the diorites were homogenous before alteration, without any significant influence of magmatic processes (e.g., partial melting and crystallization differentiation). Moreover, during the evolution of magmas, heavy Fe isotope enrichment occurs in the melt with the decrease of iron content (e.g., Foden et al., 2015; Heimann et al., 2008; Poitrasson and Freydier, 2005), which is not consistent with the present data where the diorite with low iron content is enriched in light Fe isotope. Similarly,

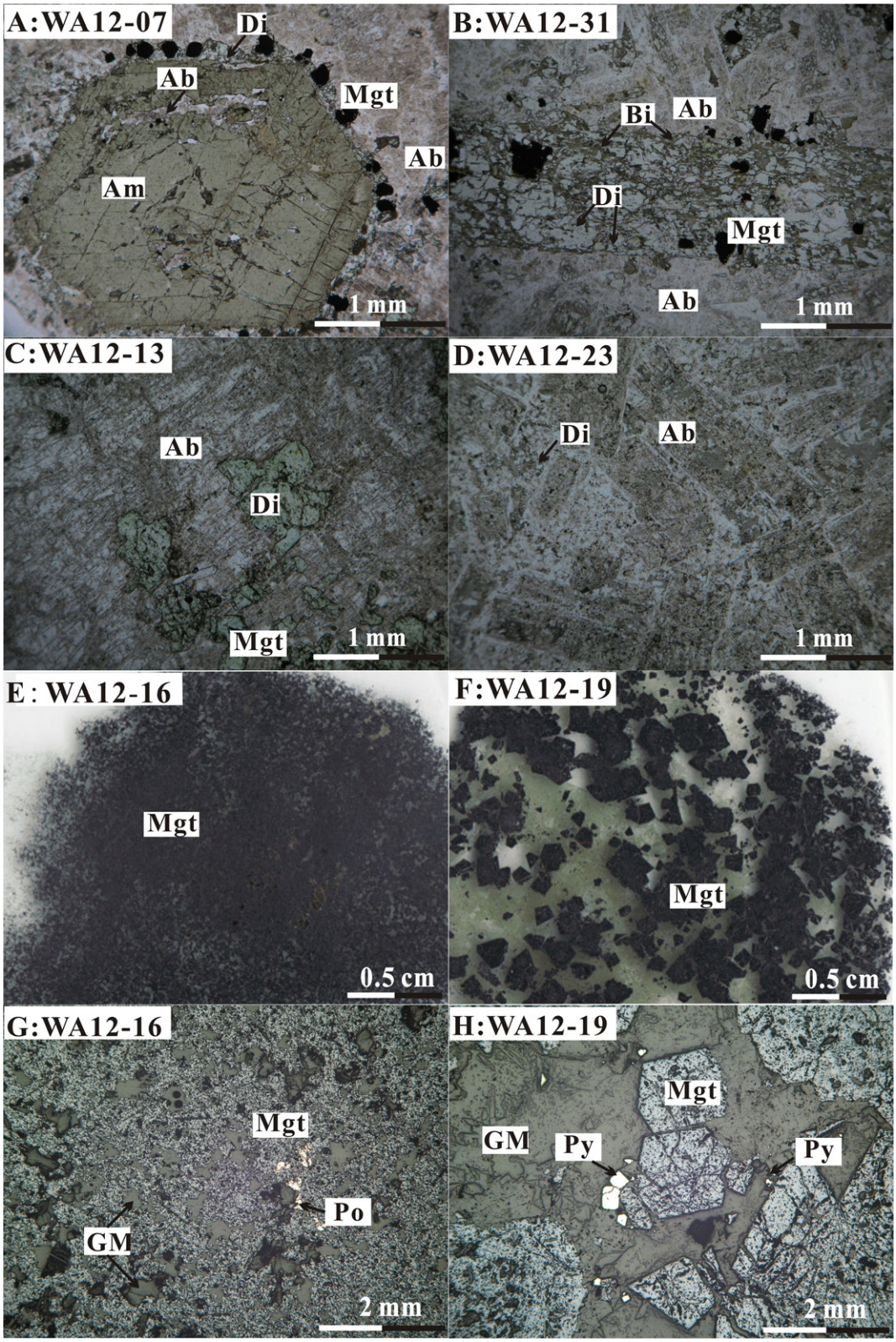

Fig. 3. Photomicorgraphs in transmitted light (A–F) and reflected light (G-H) illustrating the characteristics of altered diorites and ores from the Han-Xing iron deposit. (A) Euhedral amphibole was replaced by the diopside and albite with the formation of magnetite along the edge of the amphibole. (B) Amphibole was completely altered and replaced by the aggregates of diopside, biotite, magnetite and albite. (C) With the increase in the degree of alteration, the newly-formed diopside was further transformed to albite, showing the residual diopside surrounded by albite. (D) Extensive alteration, all the minerals were dissolved except for albite and minor diopside left as the residues. (E) Scanned image of thin section, showing the fine-grained anhedral–subhedral magnetite in ores. (F) Scanned image of thin section, showing the coarse-grained euhedral magnetite in ores. (G) Fine-grained anhedral–subhedral magnetite, gangue minerals and anhedral pyrrhotite. (H) Coarse-grained euhedral magnetite, subhedral gangue minerals and anhedral–euhedral pyrite. Abbreviations: Am-amphibole; Di-diopside; Bi-biotite; Ab-albite; Mgt-magnetite; Py-pyrite; Po-pyrrhotite; GM-gangue minerals.

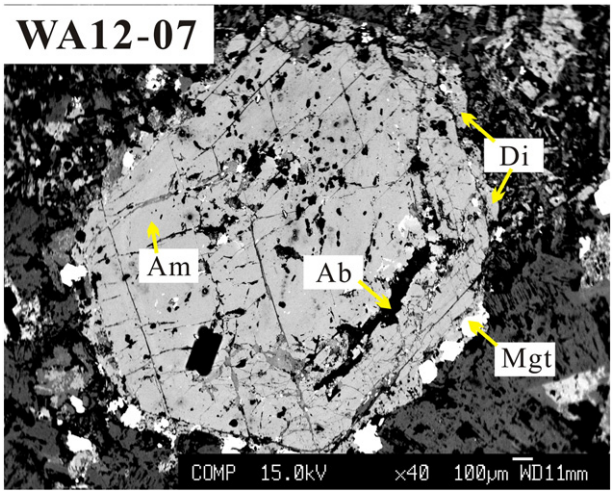

Fig. 4. The BSE image showing the reaction texture of amphibole in altered diorite (Sample WA12-07). The euhedral amphibole reacted with fluids and was replaced by the newly-formed diopside, albite and magnetite.

secondary alteration after skarn-type alteration will result in the light Fe isotope preferentially leaching from the diorites (Chapman et al., 2009; Cheng et al., 2015). Petrological observations did not reveal any significant secondary alteration in these diorites. Therefore, the large variation of $\delta^{56}Fe$ in the diorites cannot be result of early magmatic processes and late secondary alteration. The negative correlations between LOI and TFe_2O_3 from these diorites indicate that skarn-type alteration might have resulted in the Fe isotopic fractionation.

Iron and titanium have similar geochemical property in magmatic system, and therefore magmatic rocks belonging to the same suite display positive relationship between iron and titanium (Ragland, 1989). However, during the alteration process, iron is a mobile element whereas titanium is an immobile element. Therefore, TFe_2O_3/TiO_2 ratio is a good proxy for constraining the possible mobilization and transport of iron (Dauphas et al., 2004; Rouxel et al., 2003). The good correlation between $\delta^{56}Fe$ values and their TFe_2O_3/TiO_2 ratios of altered diorites demonstrates that Fe isotope fractionation might have occurred during the diorite skarn-type alteration (Fig. 7). The low TFe_2O_3/TiO_2 ratio indicates a high degree of alteration and substantial loss of iron. The most intensely altered sample WA12-23 has the lowest TFe_2O_3/TiO_2 ratio and its low $\delta^{56}Fe$ value demonstrates that heavy Fe isotopes were preferentially leached from the diorites during the skarn-type alteration.

We also note a negative correlation between Fe^{2+}/Fe^{3+} and TFe_2O_3/TiO_2 ratios of the altered diorites (Fig. 7), which indicates that the diorite skarn-type alteration heavily affected Fe^{3+} over Fe^{2+}. This is consistent with our petrological observation. When amphibole was converted to diopside, Fe^{2+} was left in the diopside but Fe^{3+} was partitioned into the newly-formed magnetite (Figs. 3A-B and 4). With the increase in the degree of alteration, both the newly-formed hydrothermal magnetite and the pre-existing magmatic magnetite were dissolved from the diorites, with albite and minor diopside left as the residue (Figs. 3C–D). Previous studies have well documented that $^{56}Fe/^{54}Fe$ will usually be higher in Fe^{3+} compounds than in Fe^{2+}-bearing species (e.g., Bullen et al., 2001; Johnson et al., 2002; Polyakov and Mineev, 2000; Schauble et al., 2001) and that magnetite is enriched in heavy Fe isotopes relative to the silicate minerals, with the fractionation factor $\Delta^{56}Fe_{Mgt-Fe\ sil}$ predicted as large as +0.25‰ (e.g. Heimann et al., 2008; Shahar et al., 2008; Telus et al., 2012). These factors explain why the heavy Fe isotopes were preferentially leached from the diorites during the skarn-type alteration.

If we assume that iron was leached from diorites following Rayleigh fractionation, the Rayleigh equation $((1000 + \delta^{56}Fe_A)/(1000 + \delta^{56}Fe_i) = F^{(\alpha B - A - 1)}$ can be applied, where A refers to the altered diorite as the residual phase, B refers to the iron leached from the diorites, i refers to the initial $\delta^{56}Fe$ values and F ($F = (TFe_2O_3/TiO_2)_A/(TFe_2O_3/TiO_2)_i$) refers to the proportion of iron in the altered diorites to the initial content. In this present case, i is represented by sample WA12-14. The fractionation factor between leached iron and altered residues has been calculated, $\alpha_{B\text{-}A}$ varies from 1.0002 to 1.0011 (Table 4). Using mass balance equation: $\delta^{56}Fe_i \approx \delta^{56}Fe_{altered\ diorite} * F + \delta^{56}Fe_{leached} * (1 - F)$, we calculated the mean Fe isotopic composition of the iron leached from the weakest altered sample WA12-14 to the most extensively altered sample WA12-23, i.e., $\delta^{56}Fe_{leached}$ is +0.381‰. The results show that the $\delta^{56}Fe$ value of the iron leached from the diorites can be 0.18‰ heavier than that of the initial diorite (Sample WA12-14).

Table 3
Major elements concentration of representative minerals in altered diorite sample WA12-07.

Comment	Am	Am	Am	Am	Am	Di	Di	Di	Ab
SiO_2	41.7	41.8	41.5	41.0	41.4	51.4	53.6	52.3	67.0
TiO_2	1.95	1.84	1.90	1.93	2.08	0.42	0.01	0.31	0.00
Al_2O_3	12.5	12.6	12.7	13.0	12.5	2.80	0.31	2.27	20.7
Cr_2O_3	0.00	0.00	0.03	0.02	0.00	0.00	0.01	0.02	0.02
FeO	13.4	13.8	13.4	15.3	14.4	9.04	9.63	8.04	0.26
MnO	0.23	0.23	0.21	0.24	0.32	0.48	0.12	0.28	0.00
MgO	12.2	12.0	12.2	10.8	11.4	12.8	12.9	13.5	0.04
CaO	11.6	11.2	11.4	11.5	11.6	22.2	21.0	22.4	0.67
NiO	0.00	0.00	0.00	0.01	0.03	0.00	0.00	0.00	0.00
Na_2O	2.47	2.38	2.42	2.28	2.38	0.65	1.71	0.31	10.6
K_2O	1.23	1.24	1.21	1.49	1.32	0.00	0.01	0.01	0.71
Total	97.3	97.1	97.0	97.6	97.3	99.8	99.3	99.3	100.0

Note: Am, amphibole; Di, diopside; Ab, albite.

Table 2
Major elements concentration of altered diorites, synetite and limestones from Han-Xing iron deposit.

Sample	WA12-07	WA12-08	WA12-13	WA12-14	WA12-23	WA12-31	WA12-14-1	WA12-10	WA12-30
Description	Altered diorite	Altered diorite	Altered diorite	Altered diorite	Altered diorite	Altered diorite	Synetite	Limestone	Limestone
SiO_2	57.6	58.2	54.1	58.5	58.3	58.3	64.3	2.94	1.15
TiO_2	0.65	0.61	0.63	0.53	0.57	0.61	0.18	0.04	0.02
Al_2O_3	16.1	17.0	16.7	17.0	17.6	17.3	17.6	0.64	0.36
TFe_2O_3	6.72	4.94	3.29	5.86	2.48	4.75	1.25	0.34	0.49
FeO	2.10	1.54	1.58	1.77	1.26	1.12	0.25	0.20	0.25
MnO	0.07	0.06	0.06	0.06	0.08	0.07	0.02	0.01	0.03
MgO	2.13	2.19	3.04	1.68	2.65	1.79	1.70	13.2	21.7
CaO	4.57	6.21	7.90	4.10	4.51	6.82	0.96	40.2	31.1
Na_2O	3.89	7.34	7.09	5.54	6.61	6.96	6.26	0.08	0.04
K_2O	6.70	0.73	1.99	4.52	3.08	1.29	5.72	0.10	0.02
P_2O_5	0.41	0.41	0.39	0.37	0.32	0.39	0.04	0.02	0.01
LOI	0.68	1.90	3.89	1.08	2.98	2.04	1.34	43.1	46.18
Total	99.6	99.5	99.0	99.2	99.1	100.3	99.4	100.7	101.1

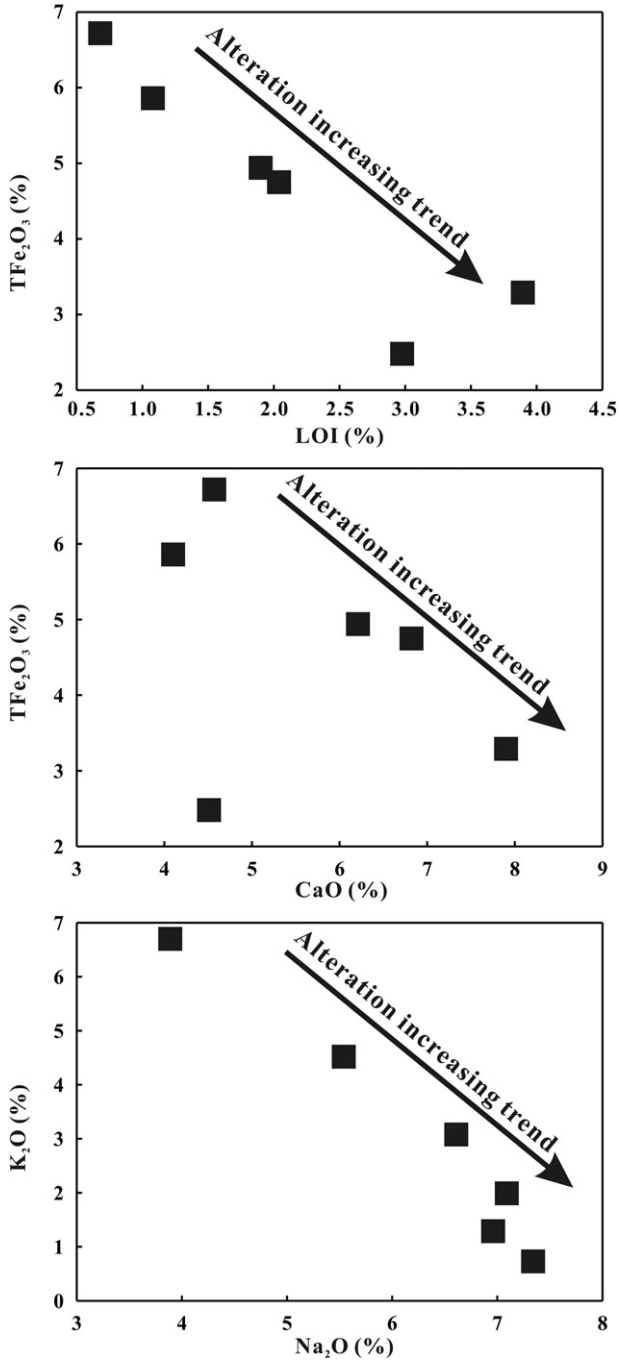

Fig. 5. TFe_2O_3 vs. LOI, TFe_2O_3 vs. CaO, and K_2O vs. Na_2O contents of altered diorites.

5.2. Fe isotope fractionation between ore minerals

Distinguishing the isotopic equilibrium among minerals is quite important for interpreting the characteristic of Fe isotope ratios. The "δ^{56}Fe–δ^{56}Fe" plot in different minerals is useful to determine whether the mineral pairs are equilibrated in Fe isotope or not. For the Han-Xing Fe skarn deposit, it appears that pyrite and pyrrhotite may attain Fe isotopic equilibrium, since a concord line with a slope of 0.78 (Fig. 8) is yielded which is close to 1. However, magnetite did not attain Fe isotopic equilibrium with pyrite and pyrrhotite as suggested by the gentle slopes of 0.24 and 0.13, respectively (Fig. 8). This means that magnetite did not re-equilibrate with the late stage sulfides. As shown in Fig. 6, magnetite spans a narrow range in δ^{56}Fe values, which excludes the possibility of kinetic fractionation (Skulan et al., 2002) and suggests that magnetite should have attained Fe isotopic equilibrium with the ore-forming fluid when it precipitated. Furthermore, the two types of magnetite with identical Fe isotopic compositions suggest an equilibrium fractionation between magnetite and ore-forming fluid.

At equilibrium conditions, the theoretical Fe isotope fractionation between minerals can be calculated using published reduced partition functions (e.g., Polyakov and Mineev, 2000; Polyakov and Soultanov, 2011). For a typical magmatic-hydrothermal temperature of 350 °C, it can be predicted as 10^3 ln β py > mgt > po, which is not completely consistent with our observation, i.e., $\delta^{56}Fe_{py} > \delta^{56}Fe_{po} > \delta^{56}Fe_{mgt}$. This inconsistency also suggests the Fe isotopic disequilibrium between magnetite and sulfides. The "δ^{56}Fe–δ^{56}Fe" plot suggests equilibrium fractionation between pyrite and pyrrhotite with a small isotopic fractionation factor (Fig. 8), whereas the predicted fractionation factor is much larger (e.g., Polyakov and Mineev, 2000). One possible explanation is that pyrite and pyrrhotite did not attain Fe isotopic equilibrium and resulted from the kinetic fractionation as reported by Syverson et al. (2013). The slope of 0.78 may be just a coincidence for the few data points. The other explanation is that pyrite and pyrrhotite attained isotopic equilibrium, but the reduced partition function of troilite is not suitable for pyrrhotite, since these minerals do not have same chemical composition and structure, although some researchers use troilite to represent pyrrhotite (e.g., Wawryk and Foden, 2014). More experimental work on the Fe isotope fractionation between pyrite and pyrrhotite are needed in future.

5.3. Metal source of the Han-Xing Fe skarn deposit

In order to use Fe isotopes to constrain the metal source of the Han-Xing Fe skarn deposit, a key point is the information on the Fe isotopic composition of ore-forming fluid. As discussed before, magnetite might have attained Fe isotopic equilibrium with the ore-forming fluid when it was deposited. Therefore, combining the Fe isotopic composition of magnetite and the equilibrium fractionation factor, it is possible to calculate the Fe isotopic composition of ore-forming fluid. Frierdich et al. (2014) used the three-isotope method to determine the equilibrium Fe isotope fractionation factor between Fe (II) solutions and magnetite and provided the experimental formula as: $10^3 \ln\alpha_{Fe\ (II)\ aq\ -\ mgt} = -0.145\ (\pm 0.002) \times 10^6/T^2 + 0.10(\pm 0.02)$, where T is in K. Fluid inclusion work by Zhang et al. (1996) in this area demonstrated that the average temperature of ore-forming fluid was 416 °C when the magnetite deposited. Thus, the calculated equilibrium Fe isotope fractionation factor between Fe (II) $_{aq}$ and magnetite, $10^3 \ln\alpha_{Fe\ (II)\ aq\ -\ mgt}$, is −0.21. Even if the magnetite did not completely equilibrate with the ore-forming fluid, it should also preferentially fractionate heavy Fe isotopes (e.g., Johnson et al., 2005; Frierdich et al., 2014). Therefore, for the Han-Xing Fe skarn deposit, the ore-forming fluid should be isotopically lighter than magnetite. Based on this conclusion, the metal source of Fe skarn deposit is addressed in the next section.

5.3.1. Recycling of pre-existing ore deposits?

Earlier studies considered the Han-Xing iron deposit as a product of recycling of sedimentary deposits by the later hydrothermal fluid (Wang et al., 1981), since the ore bodies are found in association with the Majiagou limestone although several limestone units are in contact with the plutonic rocks in this region. In addition, sulfur isotopic composition of the pyrite in ores shows a mixture of sedimentary and igneous sulfur (Shen et al., 2013).

As seen in Fig. 6, magnetite has limited δ^{56}Fe values with an average of +0.12‰. If the magnetite is a product of recycling of pre-existing sedimentary deposit, it should have a large range in δ^{56}Fe values because of the various degrees of recycling and the initial large Fe isotopic variation in sedimentary iron deposits as observed by Johnson et al. (2003). More importantly, if the iron in the earlier sedimentary deposit occurs as siderite, the newly magnetite should have similar Fe isotopic

Table 4
Fe isotopic compositions of altered diorites, syenite, limestones and mineral separates from Han-Xing iron deposit.

Sample	Description	TFe_2O_3(%)	TFe_2O_3/TiO_2	Fe^{2+}/Fe^{3+}	$\delta^{56}Fe$	2SE	$\delta^{57}Fe$	2SE	n	F	α_{B-A}
Bulk samples											
BCR-2	Basalt standard	–	–	–	0.087	0.024	0.122	0.036	9	–	–
WA12-14	Altered diorite	5.86	11.1	0.49	0.205	0.030	0.251	0.053	4	1.00	–
WA12-07	Altered diorite	6.72	10.3	0.52	0.130	0.030	0.177	0.060	4	0.94	1.0011
WA12-08	Altered diorite	4.94	8.10	0.54	0.101	0.030	0.103	0.053	4	0.73	1.0003
WA12-31	Altered diorite	4.69	7.79	0.35	0.056	0.030	0.091	0.053	4	0.70	1.0004
WA12-13	Altered diorite	3.29	5.22	1.13	0.035	0.030	0.045	0.053	4	0.47	1.0002
WA12-23	Altered diorite	2.48	4.35	1.27	−0.071	0.030	−0.171	0.053	4	0.39	1.0003
WA12-14-1	Syenite	1.25	6.90	0.22	0.181	0.030	0.215	0.053	4	–	–
WA12-10	Limestone	–	–	–	−0.102	0.030	−0.159	0.053	4	–	–
WA12-30	Limestone	–	–	–	−0.223	0.030	−0.305	0.053	4	–	–
Mineral separates											
WA12-01	Magnetite	–	–	–	0.152	0.034	0.229	0.061	4	–	–
WA12-04	Fine magnetite	–	–	–	0.207	0.034	0.271	0.061	4	–	–
WA12-16	Fine magnetite	–	–	–	0.147	0.030	0.232	0.053	4	–	–
WA12-17	Fine magnetite	–	–	–	0.102	0.030	0.170	0.053	4	–	–
WA12-19	Coarse magnetite	–	–	–	0.121	0.030	0.161	0.053	4	–	–
WA12-20	Coarse magnetite	–	–	–	0.094	0.030	0.095	0.053	4	–	–
WA12-24	Fine Magnetite	–	–	–	0.137	0.029	0.241	0.055	4	–	–
WA12-33	Fine magnetite	–	–	–	0.072	0.029	0.146	0.055	4	–	–
WA12-34	Coarse magnetite	–	–	–	0.098	0.029	0.133	0.055	4	–	–
WA12-35	Coarse magnetite	–	–	–	0.112	0.029	0.147	0.055	4	–	–
WA12-35	Fine magnetite	–	–	–	0.137	0.029	0.213	0.055	4	–	–
WA12-36	Coarse magnetite	–	–	–	0.080	0.029	0.115	0.055	4	–	–
WA12-36	Fine magnetite	–	–	–	0.115	0.029	0.129	0.055	4	–	–
WA12-37	Coarse magnetite	–	–	–	0.112	0.029	0.187	0.055	4	–	–
WA12-37P	Coarse magnetite	–	–	–	0.109	0.029	0.161	0.055	4	–	–
WA12-04	Pyrite	–	–	–	0.482	0.030	0.685	0.053	4	–	–
WA12-19	Pyrite	–	–	–	0.393	0.030	0.604	0.053	4	–	–
WA12-20	Pyrite	–	–	–	0.346	0.032	0.511	0.074	4	–	–
WA12-33	Pyrite	–	–	–	0.117	0.029	0.194	0.055	4	–	–
WA12-34	Pyrite	–	–	–	0.116	0.029	0.145	0.055	4	–	–
WA12-36	Pyrite	–	–	–	0.327	0.029	0.498	0.055	4	–	–
WA12-37	Pyrite	–	–	–	0.355	0.029	0.496	0.055	4	–	–
WA12-16	Pyrrhotite	–	–	–	0.334	0.030	0.478	0.053	4	–	–
WA12-17	Pyrrhotite	–	–	–	0.304	0.030	0.450	0.053	4	–	–
WA12-19	Pyrrhotite	–	–	–	0.353	0.030	0.483	0.053	4	–	–
WA12-24	Pyrrhotite	–	–	–	0.343	0.029	0.532	0.055	4	–	–
WA12-34	Pyrrhotite	–	–	–	0.120	0.029	0.139	0.055	4	–	–
WA12-35	Pyrrhotite	–	–	–	0.255	0.029	0.347	0.055	4	–	–
WA12-36	Pyrrhotite	–	–	–	0.281	0.029	0.402	0.055	4	–	–
WA12-37	Pyrrhotite	–	–	–	0.278	0.029	0.410	0.055	4	–	–

Note: $2SE = [(2SD_{standard}/n^{1/2})^2 + 2SE^2_{chemical\ process}]^{1/2}$, where n is the number of replicate analyses.

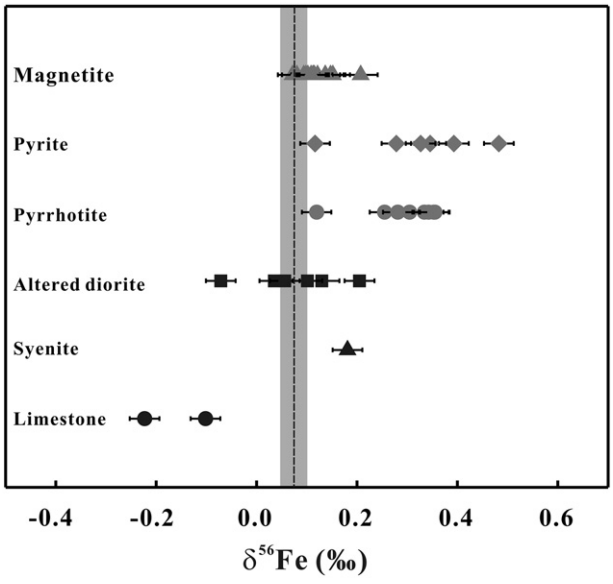

Fig. 6. $\delta^{56}Fe$ variation in different rock types and mineral separates from the Han-Xing iron deposit. The shaded area corresponds to the Fe isotopic composition (0.07 ± 0.03 and $\delta^{56}Fe$ was recalculated as $\delta^{57}Fe * 0.67$) of the mean mafic earth as defined by Poitrasson et al. (2004).

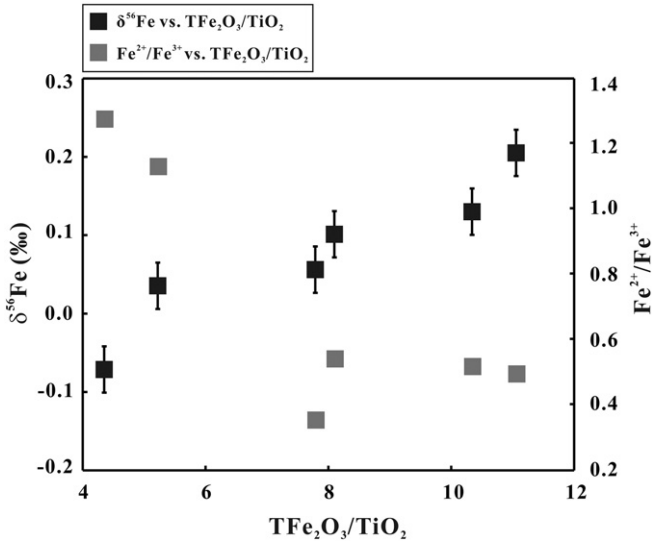

Fig. 7. $\delta^{56}Fe$ and Fe^{2+}/Fe^{3+} vs. TFe_2O_3/TiO_2 for altered diorites from the Han-Xing iron deposit.

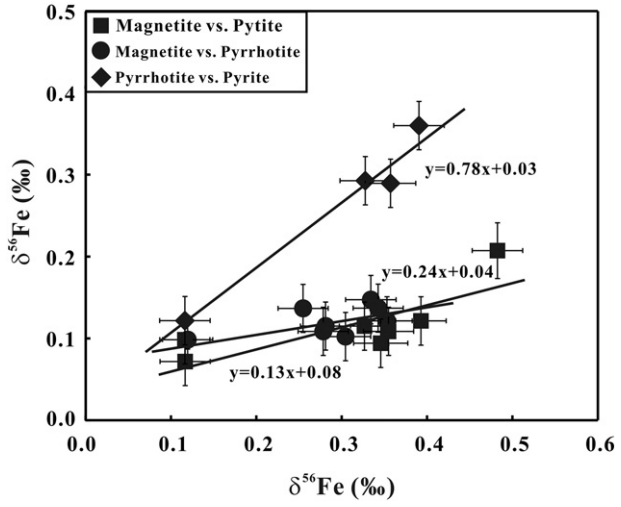

Fig. 8. Inter-mineral Fe isotope fractionation in ores from the Han-Xing iron deposit.

composition with that of siderite. Both theoretical prediction (e.g., Blanchard et al., 2009; Polyakov and Mineev, 2000) and experimental measurements (e.g., Craddock and Dauphas, 2011b; Heimann et al., 2010; Johnson et al., 2003; Markl et al., 2006; Steinhoefel et al., 2010) have demonstrated that siderite is enriched in light Fe isotope with an average δ^{56}Fe value of −0.39‰ (n = 70). Thus, the Han-Xing Fe skarn deposit cannot be the product of recycling of pre-existing sedimentary deposit.

5.3.2. Alteration of associated igneous rocks?

Alteration of associated igneous rocks, especially albitization, was also proposed for the metal sources of the Han-Xing Fe skarn deposit (e.g., Feng, 1998; Zheng et al., 2007). This model has been applied in several regions where albitization and albitite have been regarded as important signs for exploration of potential iron mineralization (Zheng et al., 2007).

At the beginning of diorite skarn-type alteration, amphibole in diorites was replaced by diopside, albite, biotite and magnetite (Figs. 3A-B and 4). With the increase in the degree of alteration, the newly formed diopside and biotite were further transferred to albite. Meanwhile the newly formed magnetite and pre-existing magmatic magnetite were dissolved from the diorites. The whole alteration process was accompanied by the removal of iron from the diorites. Whole rock geochemical data show that as much as 63% iron in the diorites might have been lost during alteration. On the other hand, EPMA data show that when amphibole, the main iron-bearing mineral in diorite, was transformed to diopside and albite, the FeO content decreases from 15.3% to 8.04% and 0.26%, respectively. In summary, substantial iron was released from the diorites during the skarn-type alteration. This raises the question whether the iron leached from diorites composed the main iron budget of the Han-Xing Fe skarn deposit.

As discussed in Section 5.1, iron leached from the diorites was enriched in heavy Fe isotopes relative to unaltered diorite. If the leached iron contributed to the main iron budget of the Han-Xing Fe skarn deposit, the ore-forming fluid should be isotopically heavier than the unaltered diorite. In this case, the magnetite which deposited from the ore-forming fluid also should be isotopically heavier than the unaltered diorite. However, this is in contradiction to our observation where the magnetite is isotopically lighter than the unaltered diorite. This demonstrates that iron leached from the diorites is not the dominant source of the Han-Xing Fe skarn deposit.

5.3.3. Magmatic hydrothermal system?

Magma plays an important role in forming hydrothermal ore deposits. It has long been recognized that cooling and crystallizing magmas may exsolve chloride-rich, metal-bearing fluids that form economic ore deposits (e.g., Candela and Holland, 1984; Eugster, 1985; Lindgren, 1906; Richards, 2003). Magmatic fluid is the primary source for hydrothermal ore deposits (Hedenquist and Lowenstern, 1994; Baker et al., 2004). However, there is still considerable debate about the extent to which the magma contributes water, metals, ligands and other components to the hydrothermal system (Hedenquist and Lowenstern, 1994), especially to the metals for which there are no direct isotope tracers.

Our observation shows that magnetite in ores is enriched in light Fe isotope relative to unaltered diorite. Combining the −0.21‰ equilibrium Fe isotope fractionation factor between Fe (II) $_{aq}$ and magnetite, the ore-forming fluid should be isotopically much lighter than the unaltered diorite. Before the magnetite deposited from the ore-forming fluid, part of iron which is isotopically heavy was added into the initial fluid, since heavy Fe isotopes were preferentially leached from the diorites during skarn-type alteration. Thus, the initial fluid might have been enriched in light Fe isotope with high iron content in order to overcome the effect of leaching of diorites and to maintain its original Fe isotopic composition.

The H and O isotope analyses of fluid inclusions contained in the hydrothermal minerals from the Han-Xing skarn deposit demonstrate that magmatic water dominates the ore-forming fluid (Zheng et al., 2007). It has been well documented that ferrous Fe-chloride complexes are the dominant iron-bearing species in magmatic fluids (e.g., Chou and Eugster, 1977; Fein et al., 1992; Simon et al., 2004; Saunier et al., 2011). Therefore, theoretically, the magmatic fluids will preferentially fractionate the light Fe isotope. Poitrasson and Freydier (2005) and Heimann et al. (2008) have speculated that magmatic fluid exsolved from host magma is enriched in light Fe isotope relative to silicate melt in order to explain the origin of high-^{56}Fe/^{54}Fe igneous rocks. This hypothesis was also supported by the positive correlation between δ^{56}Fe and δ^{66}Zn values of the pegmatites and many granitoids (Telus et al., 2012). Moreover, magmatic fluids can have high iron content as large as 9.3 wt.% measured from fluid samples and fluid inclusions (Yardley, 2005 and references therein). We therefore infer that magmatic fluid might have been the initial fluid with high iron content and light Fe isotope enrichment. Although the wall rock limestone is also isotopically lighter than the unaltered diorite (Fig. 6), its contribution to the Han-Xing Fe skarn deposit should be insignificant because of its low iron content (Table 2). Here we propose that the main iron budget of the Han-Xing Fe skarn deposit is the magmatic fluid which was exsolved from the associated intermediate magma.

6. Conclusions

Large Fe isotopic variation has been observed from the Han-Xing Fe skarn deposit. The associated limestone is isotopically lighter than the altered diorites. Sulfides (pyrite and pyrrhotite) are isotopically heavier than the magnetite. The limited Fe isotopic composition of magnetite suggests equilibrium fractionation between magnetite and ore-forming fluid. The "δ^{56}Fe–δ^{56}Fe" plot indicates that magnetite did not equilibrate with the pyrite and pyrrhotite, and suggests equilibrium fractionation between pyrite and pyrrhotite with a small fractionation factor. However, this fractionation factor is not consistent with the theoretical prediction, which can be explained by either the disequilibrium between pyrite and pyrrhotite or the inappropriate representation of troilite for the pyrrhotite.

The large Fe isotopic variation and positive correlation between δ^{56}Fe values and TFe_2O_3/TiO_2 ratios in altered diorites demonstrate that Fe isotopes indeed fractionated and that the heavy Fe isotopes were preferentially leached from the diorites during the skarn-type alteration. However, magnetite in ores is isotopically lighter than the unaltered diorite. This reveals that the leached iron did not constitute the main Fe source for the Han-Xing Fe skarn deposit although the petrological and major element investigations demonstrate that

massive iron was leached from the diorites during alteration. Our results support the hypothesis that magmatic fluid is isotopically lighter than the source intrusion. Moreover, magmatic fluid provides the dominant iron budget of the Han-Xing Fe skarn deposit.

Our work provides a good example for the application of Fe isotopes to constrain the metal source of ore deposit through detailed studies on Fe isotope fractionation. The magmatic hydrothermal ore deposits results from a complex physicochemical system leading to the formation and/or dissolution of many minerals. Therefore, further studies applying the new technology for in-situ Fe isotope measurement in minerals combined with fluid inclusions would provide further insights into Fe isotope fractionation and its implications on various geological processes.

Acknowledgments

We are grateful to J.F. Ying and Y. Sun for their assistance in the field work and B.X. Su and P.F. Zhang for helpful discussions. Professor M. Santosh is grateful to his careful revision which greatly improved English expression. Two anonymous reviewers are gratefully appreciated for their constructive comments and Prof. Huayong Chen is thanked for his efficient editorial handling. This research is financially supported by the Natural Science Foundation of China (Grant 91014007, 91214203 and 941173044).

References

Baker, T., van Achterberg, E., Ryan, C.G., Lang, J.R., 2004. Composition and evolution of ore fluids in a magmatic-hydrothermal skarn deposit. Geology 32, 117–120.

Beard, B.L., Johnson, C.M., 2004. Fe Isotope Variations in the Modern and Ancient Earth and Other Planetary Bodies. In: Johnson, C.M., Beard, B.L., Albarede, F. (Eds.), Geochemistry of Non-Traditional Stable IsotopesRev. Mineral. Geochem. Mineralogical Society of America and Geochemical Society, Washington DC, pp. 319–357.

Blanchard, M., Poitrasson, F., Meheut, M., Lazzeri, M., Mauri, F., Balan, E., 2009. Iron isotope fractionation between pyrite (FeS_2), hematite (Fe_2O_3) and siderite ($FeCO_3$): a first-principles density functional theory study. Geochim. Cosmochim. Acta 73, 6565–6578.

Bullen, T.D., White, A.F., Childs, C.W., Vivet, D.V., Schultz, M.S., 2001. Demonstration of significant abiotic iron isotope fractionation in nature. Geology 29, 699–702.

Candela, P.A., Holland, H.D., 1984. The partitioning of copper and molybdenum between silicate melts and aqueous fluids. Geochim. Cosmochim. Acta 48, 373–380.

Chapman, J.B., Weiss, D.J., Shan, Y., Lemburger, M., 2009. Iron isotope fractionation during leaching of granite and basalt by hydrochloric and oxalic acids. Geochim. Cosmochim. Acta 73, 1312–1324.

Chen, B., Jahn, B.M., Arakawa, Y., Zhai, M.G., 2004. Petrogenesis of the Mesozoic intrusive complexes from the southern Taihang Orogen, North China craton: elemental and Sr-Nd-Pb isotopic constraints. Contrib. Mineral. Petrol. 148, 489–501.

Chen, B., Tian, W., Jahn, B.M., Chen, Z.C., 2008. Zircon SHRIMP U-Pb ages and in-situ Hf isotopic analysis for the Mesozoic intrusions in South Taihang, North China Craton: evidence for hybridization between mantle-derived magmas and crustal components. Lithos 102, 118–137.

Cheng, Y., Mao, J., Zhu, X., Wang, Y., 2015. Iron isotope fractionation during supergene weathering process and its application to constrain ore genesis in Gaosong deposit, Gejiu district, SW China. Gondwana Res. 27, 1283–1291.

Chou, I.M., Eugster, H.P., 1977. Solubility of magnetite in supercritical chloride solutions. Am. J. Sci. 277, 1296–1314.

Craddock, P.R., Dauphas, N., 2011a. Iron isotopic compositions of geological reference materials and chondrites. Geostand. Geoanal. Res. 35, 101–123.

Craddock, P.R., Dauphas, N., 2011b. Iron and carbon isotope evidence for microbial iron respiration throughout the Archean. Earth Planet. Sci. Lett. 303, 121–132.

Dauphas, N., Pourmand, A., Teng, F.Z., 2009. Routine isotopic analysis of iron by HR-MC-ICPMS: how precise and how accurate? Chem. Geol. 267, 175–184.

Dauphas, N., van Zuilen, M., Wadhwa, M., Davis, A.M., Marty, B., Janney, P.E., 2004. Clues from Fe isotope variations on the origin of early Archean BIFs from Greenland. Science 306, 2077–2080.

Dideriksen, K., Baker, C.A., Stipp, S.L.S., 2006. Iron isotopes in natural carbonate minerals determined by MC-ICP-MS with a ^{58}Fe–^{54}Fe double spike. Geochim. Cosmochim. Acta 70, 118–132.

Eugster, H.P., 1985. Granites and hydrothermal ore-deposits — a geochemical framework. Mineral. Mag. 49, 7–23.

Fein, J.B., Hemley, J.J., D'Angelo, W.M., Komninou, A., Svergensky, D.A., 1992. Experimental study of iron-chloride complexing in hydrothermal fluids. Geochim. Cosmochim. Acta 56, 3179–3190.

Feng, Z.Y., 1998. Comparison of iron skarn generating intrusions with barren intrusions in southern taihang mountain, China. Geosciences 1, 467–476 (in Chinese with English abstract).

Foden, J., Sossi, P.A., Wawryk, C.M., 2015. Fe isotopes and the contrasting petrogenesis of A-, I- and S-type granite. Lithos 212-215, 32–44.

Frierdich, A.J., Beard, B.L., Scherer, M.M., Johnson, C.L., 2014. Determination of the $Fe(II)_{aq}$-magnetite equilibrium iron isotope fractionation factor using the three-isotope method and a multi-direction approach to equilibrium. Earth Planet. Sci. Lett. 391, 77–86.

Graham, S., Pearson, N., Jackson, S., Griffin, W., O'Reilly, S.Y., 2004. Tracing Cu and Fe from source to porphyry: in situ determination of Cu and Fe isotope ratios in sulfides from the Grasberg Cu-Au deposit. Chem. Geol. 207, 147–169.

He, Y.S., Ke, S., Teng, F.Z., Wang, T.T., Wu, H.J., Liu, S.A., Lu, Y.H., Li, S.G., 2015. High precision iron isotope analysis of geological reference materials by high resolution MC-ICP-MS. Geostand. Geoanal. Res. 39, 341–356.

Hedenquist, J.W., Lowenstern, J.B., 1994. The role of magmas in the formation of hydrothermal ore deposits. Nature 370, 519–527.

Heimann, A., Beard, B.L., Johnson, C.M., 2008. The role of volatile exsolution and subsolidus fluid/rock interactions in producing high $^{56}Fe/^{54}Fe$ ratios in siliceous igneous rocks. Geochim. Cosmochim. Acta 72, 4379–4396.

Heimann, A., Johnson, C.M., Beard, B.L., Valley, J.W., Roden, E.E., Spicuzza, M.J., Beukes, N.J., 2010. Fe, C, and O isotope compositions of banded iron formation carbonates demonstrate a major role for dissimilatory iron reduction in ~2.5 Ga marine environments. Earth Planet. Sci. Lett. 294, 8–18.

Icopini, G.A., Anbar, A.D., Ruebush, S.S., Tien, M., Brantley, S.L., 2004. Iron isotope fractionation during microbial reduction of iron: the importance of adsorption. Geology 32, 205–208.

Jia, Y., Kerrich, R., 1999. Nitrogen isotope systematics of mesothermal lode gold deposits: metamorphic, granitic, meteoric water, or mantle origin? Geology 27, 1051–1054.

Jin, Z.L., Zhang, Z.C., Hou, T., Santosh, M., Han, L., 2015. Genetic relationship of high-Mg dioritic pluton to iron mineralization: a case study from the Jinling skarn-type iron deposit in the north China craton. J. Asian Earth Sci. http://dx.doi.org/10.1016/j.jseaes.2015.03.039.

Johnson, C.M., Beard, B.L., Beukes, N.J., Klein, C., O'Leary, J.M., 2003. Ancient geochemical cycling in the Earth as inferred from Fe isotope studies of banded iron formations from the Transvaal craton. Contrib. Mineral. Petrol. 144, 523–547.

Johnson, C.M., Roden, E.E., Welch, S.A., Beard, B.L., 2005. Experimental constraints on Fe isotope fractionation during magnetite and Fe carbonate formation coupled to dissimilatory hydrous ferric oxide reduction. Geochim. Cosmochim. Acta 69 (4), 963–993.

Johnson, C.A., Rye, D.M., Skinner, B.J., 1990. Petrology and stable isotope geochemistry of the metamorphosed zinc-iron-manganese deposit at sterling hill, New Jersey. Econ. Geol. 85, 1133–1161.

Johnson, C.M., Skulan, J.L., Beard, B.L., Sun, H., Nealson, K.H., Braterman, P.S., 2002. Isotopic fractionation between Fe (III) and Fe (II) in aqueous solutions. Earth Planet. Sci. Lett. 195, 141–153.

Li, L.M., 1986. A discussion on the ore-control structure factors of the Han-Xing iron deposit. Geophys. Prospect. 22, 1–11 (in Chinese).

Lindgren, W., 1906. Ore deposition and deep mining. Econ. Geol. 1, 34–46.

Markl, G., von Blanckenbur, F., Wagner, T., 2006. Iron isotope fractionation during hydrothermal ore deposition and alteration. Geochim. Cosmochim. Acta 70, 3011–3030.

Meinert, L.D., Dipple, G.M., Nicolescu, S., 2005. World skarn deposits. Econ. Geol. 100, 299–336.

Ohmoto, H., 1972. Systematics of sulfur and carbon isotopes in hydrothermal ore deposit. Econ. Geol. 67, 551–578.

Poitrasson, F., Freydier, R., 2005. Heavy iron isotope composition of granites determined by high resolution MC-ICP-MS. Chem. Geol. 222, 132–147.

Poitrasson, F., Halliday, A.N., Lee, D.C., Levasseur, S., Teutsch, N., 2004. Iron isotope differences between Earth, Moon, Mars and Vesta as possible records of contrasted accretion mechanisms. Earth Planet. Sci. Lett. 223, 253–266.

Polyakov, V.B., Mineev, S.D., 2000. The use of Mössbauer spectroscopy in stable isotope geochemistry. Geochim. Cosmochim. Acta 64, 849–865.

Polyakov, V.B., Soultanov, D.M., 2011. New data on equilibrium iron isotope fractionation among sulfides: constraints on mechanisms of sulfide formation in hydrothermal and igneous system. Geochim. Cosmochim. Acta 75, 1957–1974.

Qian, Q., Hermann, J., 2010. Formation of high-Mg diorites through assimilation of peridotite by monzodiorite magma at crustal depths. J. Petrol. 51, 1381–1416.

Ragland, P.C., 1989. Basic Analytical Petrology. Oxford University Press.

Richards, J.P., 2003. Tectono-magmatic precursors for porphyry Cu–(Mo–Au) deposit formation. Econ. Geol. 98, 1515–1533.

Rouxel, O., Dobbek, N., Ludden, J., Fouquet, Y., 2003. Iron isotope fractionation during oceanic crust alteration. Chem. Geol. 202, 155–182.

Rye, R.O., 1966. The carbon, hydrogen, and oxygen isotopic composition of the hydrothermal fluids responsible for the lead-zinc deposits at Providencia, Zacatecas, Mexico. Econ. Geol. 61, 1399–1427.

Santosh, M., Yang, Q.Y., Teng, X.M., Tang, L., 2015. Paleoproterozoic crustal growth in the North China Craton: evidence from the LÜliang complex. Precambrian Res. 263, 197–231.

Saunier, G., Pokrovski, G.S., Poitrasson, F., 2011. First experimental determination of iron isotope fractionation between hematite and aqueous solution at hydrothermal conditions. Geochim. Cosmochim. Acta 75, 6629–6654.

Schauble, E.A., Rossman, G.R., Taylor Jr., H.P., 2001. Theoretical estimates of equilibrium Fe-isotope fractionations from vibrational spectroscopy. Geochim. Cosmochim. Acta 65, 2487–2497.

Shahar, A., Young, E.D., Manning, C.E., 2008. Equilibrium high-temperature Fe isotope fractionation between fayalite and magnetite: an experimental approach. Earth Planet. Sci. Lett. 268, 330–338.

Shen, J.F., Santosh, M., Li, S.R., Zhang, H.F., Yin, N., Dong, G.C., Wang, Y.J., Ma, G.G., Yu, H.J., 2013. The beiminghe skarn iron deposit, eastern China: geochronology, isotope geochemistry and implications for the destruction of the North China Craton. Lithos 156-159, 218–229.

Sheppard, S.M.F., Nielsen, R.L., Taylor, H.P., 1971. Hydrogen and oxygen isotope ratios in minerals from porphyry copper deposits. Econ. Geol. 66, 515–542.

Shimazaki, H., 1980. Characteristics of skarn deposits and related acid magmatism in Japan. Econ. Geol. 75, 173–183.
Simon, A.C., Pettke, T., Candela, P.A., Piccoli, P.M., Heinrich, C.A., 2004. Magnetite solubility and iron transport in magmatic-hydrothermal environments. Geochim. Cosmochim. Acta 68, 4905–4914.
Skulan, J.L., Beard, B.L., Johnson, C.M., 2002. Kinetic and equilibrium Fe isotope fractionation between aqueous Fe (III) and hematite. Geochim. Cosmochim. Acta 66, 2995–3015.
Steinhoefel, G., von Blanckenburg, F., Horn, I., Konhauser, K.O., Beukes, N.J., Gutzmer, J., 2010. Deciphering formation processes of banded iron formations from the Transvaal and the Hamersley successions by combined Si and Fe isotope analysis using UV femtosecond laser ablation. Geochim. Cosmochim. Acta 74, 2677–2696.
Syverson, D.D., Borrok, D.M., Seyfried, W.E., 2013. Experimental determination of equilibrium Fe isotopic fractionation between pyrite and dissolved Fe under hydrothermal conditions. Geochim. Cosmochim. Acta 122, 170–183.
Taylor, H.P., 1974. The application of oxygen and hydrogen isotope studies to problems of hydrothermal alteration and ore deposition. Econ. Geol. 69, 843–883.
Telus, M., Dauphas, D., Moynier, F., Tissot, F., Teng, F., Nabelek, P., Craddock, P., Groat, L., 2012. Iron, zinc, magnesium and uranium isotopic fractionation during continental crust differentiation: the tale from migmatites, granitoids and pegmatites. Geochim. Cosmochim. Acta 97, 247–265.
Teng, F.Z., Dauphas, N., Helz, R.T., 2008. Iron isotope fractionation during magmatic differentiation in Kilauea Iki Lava Lake. Science 320, 1620–1622.
Wang, Y.L., Ren, F.G., Shi, Y., 1981. Discuss the iron source and origin of the iron ore deposit of Hanxing type. Bull. Tianjin Inst. Geol. M.R. 3, 1–10 (in Chinese with English abstract).
Wang, Y., Zhu, X.K., Mao, J.W., Li, Z.H., Cheng, Y.B., 2011. Iron isotope fractionation during skarn-type metallogeny: a case study of Xinqiao Cu-S-Fe-Au deposit in the middle-lower Yangtze valley. Ore Geol. Rev. 43, 194–202.
Wawryk, C.M., Foden, J.D., 2014. Fe-isotope fractionation in magmatic-hydrothermal mineral deposits: a case study from the Renison Sn–W deposit, Tasmania. Geochim. Cosmochim. Acta 150, 285–298.
Xie, Q.H., Zhang, Z.C., Hou, T., Santosh, M., Jin, Z.L., Han, L., Cheng, Z.G., 2015. Petrogenesis of the Zhangmatun gabbro in the Ji'nan complex, North China Craton: implications for skarn-type iron mineralization. J. Asian Earth Sci. http://dx.doi.org/10.1016/j.jseaes.2015.03.039.
Yang, Q.Y., Santosh, M., 2015. Paleoproterozoic arc magmatism in the North China Craton: no siderian global plate tectonic shutdown. Gondwana Res. 28, 82–105.
Yang, Q.Y., Santosh, M., Collins, A.S., Teng, X.M., 2015. Microblock amalgamation in the north China craton: evidence from neoarchaean magmatic suite in the western margin of the jiaoliao block. Gondwana Res. http://dx.doi.org/10.1016/j.gr.2015.04.002.
Yardley, B.W.D., 2005. Metal concentrations in crustal fluids and their relationship to ore formation. Econ. Geol. 100, 613–632.
Young, E.D., Galy, A., Nagahara, H., 2002. Kinetic and equilibrium mass-dependent isotope fractionation laws in nature and their geochemical and cosmochemical significance. Geochim. Cosmochim. Acta 66, 1095–1104.
Zhai, M.G., 2014. Multi-stage crustal growth and cratonization of the North China Craton. Geosci. Front. 5, 457–469.
Zhai, M.G., Santosh, M., 2011. The early Precambrian odyssey of the North China Craton: a synoptic overview. Gondwana Res. 20, 6–25.
Zhang, Z.C., Hou, T., Li, H.M., Li, J.W., Zhang, Z.H., Song, X.Y., 2014b. Enrichment mechanism of iron in magmatic-hydrothermal system. Acta Petrol. Sin. 30, 1189–1204 (in Chinese with English abstract).
Zhang, Z.C., Hou, T., Santosh, M., Li, H.M., Li, J.W., Zhang, Z.H., Song, X.Y., Wang, M., 2014a. Spatio-temporal distribution and tectonic settings of the major iron deposits in China: an overview. Ore Geol. Rev. 57, 247–263.
Zhang, B.M., Zhao, G.L., Ma, G.X., 1996. The Metallogenic Series and Models of the Main Metallogenic Zones in Hebei Province. Petroleum Industry Press, pp. 1–273.
Zhao, G.C., Zhai, M.G., 2013. Lithotectonic elements of Precambrian basement in the North China Craton: review and tectonic implications. Gondwana Res. 23, 1207–1240.
Zhao, G.C., Sun, M., Wilde, S.A., Li, S.Z., 2005. Late Archean to Paleoproterozoic evolution of the North China Craton: key issues revisited. Precambrian Res. 136, 177–202.
Zheng, J.M., Mao, J.W., Chen, M.H., Li, G.D., Ban, C.Y., 2007. Geological characteristics and metallogenic model of skarn iron deposits in the Handan-Xingtai area, southern Hebei, China. Geol. Bull. China 26, 150–154 (in Chinese with English abstract).
Zhu, X.K., Guo, Y.L., Williams, R.J.P., O'Nions, R.K., Matthews, A., Belshaw, N.S., Canters, G.W., de Waal, E.C., Weser, U., Burgess, B.K., Salvato, B., 2002. Mass fractionation processes of transition metal isotopes. Earth Planet. Sci. Lett. 200, 47–62.